0273-2289/1559-0291 (Online)/07/141:51–76/$30.00

# Structure–Function Relationships of a Catalytically Efficient β-D-Xylosidase

**Douglas B. Jordan,*[,1] Xin-Liang Li,[1] Christopher A. Dunlap,[2] Terence R. Whitehead,[1] and Michael A. Cotta[1]**

*[1]Fermentation Biotechnology Research Unit, National Center for Agricultural Utilization Research, U.S. Department of Agriculture, Agricultural Research Service,[†] 1815 N. University Street, Peoria, IL 61604, E-mail: jordand@ncaur.usda.gov;*
*[2]Crop Bioprotection Research Unit, National Center for Agricultural Utilization Research, U.S. Department of Agriculture, Agricultural Research Service, 1815 N. University Street, Peoria, IL 61604*

**Received May 22, 2006; Revised July 6, 2006; Accepted July 11, 2006**

## Abstract

β-D-Xylosidase from *Selenomonas ruminantium* is revealed as the best catalyst known ($k_{cat}$, $k_{cat}/K_m$) for promoting hydrolysis of 1,4-β-D-xylooligosaccharides. $^1$H nuclear magnetic resonance experiments indicate the family 43 glycoside hydrolase acts through an inversion mechanism on substrates 4-nitrophenyl-β-D-xylopyranoside (4NPX) and 1,4-β-D-xylobiose (X2). Progress curves of 4-nitrophenyl-β-D-xylobioside, xylotetraose and xylohexaose reactions indicate that one residue from the nonreducing end of substrate is cleaved per catalytic cycle without processivity. Values of $k_{cat}$ and $k_{cat}/K_m$ decrease for xylooligosaccharides longer than X2, illustrating the importance to catalysis of subsites –1 and +1 and the lack there of subsite +2. Homology models of the enzyme active site with docked substrates show that subsites beyond –1 are blocked by protein and subsites beyond +1 are not formed; they suggest that D14 and E186 serve catalysis as general base and general acid, respectively. Individual mutations, D14A and E186A, erode $k_{cat}$ and $k_{cat}/K_m$ by $<10^3$ and to a similar extent for substrates 4NPX and 4-nitrophenyl-α-L-arabinofuranoside

[†]The mention of firm names or trade products does not imply that they are endorsed or recommended by the US Department of Agriculture over other firms or similar products not mentioned.

*Author to whom all correspondence and reprint requests should be addressed.

(4NPA), indicating that the two substrates share the same active site. With 4NPX and 4NPA, pH governs $k_{cat}/K_m$ with p$K_a$ values of 5.0 and 7.0 assigned to D14 and E186, respectively. $k_{cat}$(4NPX) has a p$K_a$ value of 7.0 and $k_{cat}$(4NPA) is pH independent above pH 4.0, suggesting that the catalytically inactive, "dianionic" enzyme form ($D14^-E187^-$) binds 4NPX but not 4NPA.

**Index Entries:** Glycoside hydrolase; stereochemistry; substrate specificity; xylan; arabinofuranosidase.

## Introduction

β-D-Xylosidase (EC 3.2.1.37) catalyzes hydrolysis of β-1,4 glycosidic bonds linking D-xylose residues *(1–9)*. Additionally, the enzyme may catalyze hydrolysis of sugar side chains (e.g., L-arabinofuranose) that can decorate xylooligosaccharide backbones. In concert with β-xylanases, which cleave larger polymers of xylose (xylans) to xylooligosaccharides, and enzymes needed to cleave sugar and acid side chains of the xylose polymer, β-xylosidase serves in the carbon cycle to degrade xylan, a major component of plant cell walls and one of the most abundant biopolymers on earth, to its monomers. Aside from its role in nature, β-xylosidase, along with other glycohydrolases, has attained prominence for use in biomedical research and industrial applications, the latter of which includes the goal of complete saccharification of xylans to monosaccharides for fermentation to fuel ethanol and other bioproducts.

Certain strains of the ruminal anaerobic bacterium, *Selenomonas ruminantium*, have been shown to enhance utilization of xylooligosaccharides under fermentation conditions *(10–12)*. Crude preparations of β-xylosidase from *S. ruminantium* GA192 (SXA), cloned and expressed in *Escherichia coli*, were shown to act on both 4-nitrophenyl-β-D-xylopyranoside (4NPX) and 4-nitrophenyl-α-L-arabinofuranoside (4NPA) with a 10-fold preference for the former substrate over the latter *(13)*. Moreover, natural oligosaccharides, produced from incubating oatspelt xylan and wheat arabinoxylan with a β-xylanase, were accepted as substrates by the preparation of SXA and converted to smaller xylooligosaccharides, xylose and arabinose *(13)*. Mechanistically interesting, potentially practical activities of SXA and the recent appearance of several X-ray structures of β-xylosidase from GH43 in the Protein Data Bank (http://www.pdb.org/) prompted structure–function studies of the enzyme reported here. Our discovery that the homogeneous SXA is the best catalyst known for promoting hydrolysis of xylooligosaccharides has practical significance, considering the millions of tons of xylan-containing biomass that could become available for industrial fermentation if highly efficient catalysts were available for saccharification. Details of SXA structure–function properties assume practical importance in the event SXA requires protein-engineering modifications for improved performance under large-scale conditions. Moreover, the studies on SXA build upon the sparse information relating structure to function in glycoside hydrolase family 43 (GH43) enzymes, particularly those that possess both xylosidase and arabinofuranosidase activities.

## Materials and Methods

### *Materials and General Methods*

Buffers, 4-nitrophenol (4NP), 4NP glycosides, and D-xylose (X1) were obtained from Sigma-Aldrich. 1,4-β-d-Xylobiose (X2), 1,4-β-D-xylotriose (X3), 1,4-β-D-xylotetraose (X4), 1,4-β-D-xylopentaose (X5), 1,4-β-D-xylohexaose (X6), and 1,5-α-L-arabinobiose (A2) were from Megazyme. 4-Nitrophenyl-β-D-xylobioside (4NPX2) was a generous gift from Dr. Peter Biely. Water was purified through a Milli-Q unit (Millipore). All other reagents were reagent grade and high purity. Kinetic viscosity measurements were made at 25°C using a Cannon-Fenske tube (Kimble); rates of sucrose solutions were divided by rates of water to yield relative viscosity ($\eta/\eta_o$). A Cary 50 Bio UV-Visible spectrophotometer (Varian), equipped with a thermostatted holder for cuvets, was used for spectral and kinetic determinations. A model SX.18MV-R stopped-flow (Applied Photophysics) was used for rapid kinetic studies. Kinetic simulations were through the computer program KINSIM: Chemical Kinetics Simulation System, 32-bit DOS-Extended Version 4.0, March, 1997 *(14)*. Manipulations of coordinates (overlays, distance measurements, etc.) were through Swiss–PDB Viewer 3.7 (http://www.expasy.org/spdbv/) *(15)*. Molecular graphics images were produced using the UCSF Chimera package from the Resource of Biocomputing, Visualization, and Informatics at the University of California, San Francisco (supported by NIH P41 RR–01081) *(16)* containing a package for calculating solvent-excluded molecular surfaces *(17)*.

### *Preparation of Homogeneous SXA and Mutant Enzymes*

Site-directed mutagenesis was performed using the QuikChange site-directed mutagenesis kit (Stratagene) according the manufacturer's instructions. Oligonucleotide primers are listed in Table 1. The template was pSRA1 with the SXA gene cloned into pET21(+) *(13)*. Complete sequences were determined on a 3700 sequencer (Applied Biosystems) using T7 promoter and specific primers to confirm that only the intended mutations had been introduced. Lasergene software (DNAStar) was used to analyze the sequence data. pSRA1 and its mutated plasmids were used for the transformation of *E. coli* BL21(DE3). Transformants were inoculated to 50 mL Luria-Bertani (LB) broth supplemented with 50 μg ampicillin/mL and the flask was shaken overnight at 250 rpm and 37°C. Twenty milliliters of the overnight culture were transferred to a 2.8-L baffled flask containing 1.0 liter SOB medium (2.0% tryptone, 0.5% yeast extract, 0.05% NaCl, 0.0186% KCl [all in wt/vol] and 10 m*M* $MgSO_4$) supplemented with 50 μg ampicillin/mL. The culture was shaken at 250 rpm and 37°C. When absorbance at 600 nm reached 0.6, the culture was brought to 1 m*M* isopropyl-β-d-thiogalactopyranoside to induce expression of the SXA gene, and shaking was continued for 4 h. Cells were harvested by centrifugation and cell pellets were stored at –80°C until use.

Table 1
Primers Used for Site-Directed Mutagenesis of SXA[a]

| Mutation | Primer sequence (5′→3′) |
|---|---|
| D14A | GGCTTTAACCCCGCCCCAGCATTGTC<br>GACAATGCTGGGGCGGGGTTAAAGCC |
| D127A | CGGTGCTGGCTTTGCAGCCTCCCTGTTCC<br>GGAACAGGGAGGCTGCAAAGCCAGCACCG |
| E186A | GATATTGCCTATACCGCCGGTCCCCACCTTTAC<br>GTAAAGGTGGGGACCGGCGGTATAGGCAATATC |
| H248A | CCCTGCAGAAATGCGGCGCAGCATCATTAGTCGAAACGC<br>GCGTTTCGACTAATGATGCTGCGCCGCATTTCTGCAGGG |
| R290A | TGTCCGCTGGGCGCAGAAACCGCCATCCA<br>TGGATGGCGGTTTCTGCGCCCAGCGGACA |

[a]Underlined nucleotides indicate mutations incorporated into primers.

Initial purification steps and diafiltration steps were performed at 4°C. Chromatography was at room temperature (~24°C). Cells were thawed, suspended in 40 mL of 50 m*M* Tris-HCl, pH 7.5 (Buffer A) containing Complete protease inhibitor cocktail (Roche), and disrupted by sonication. Following centrifugation, the supernatant was brought to 30% saturation with respect to ammonium sulfate and centrifuged. The supernatant was injected onto a column (2.6×22 cm) containing Phenyl Sepharose 6 Fast Flow resin (Amersham) equilibrated with Buffer A with 30% saturation ammonium sulfate. The column was washed until absorbance at 280 nm of the eluate became minimal (~200 mL) and developed with a 500-mL linear gradient (Buffer A + 30% saturated ammonium sulfate to Buffer A). Column fractions (7 mL) were assayed for SXA activity (Methods A or B, below) for wild-type enzyme or by sodium dodecyl sulfate (SDS)-polyacrylamide gel electrophoresis (PAGE) for catalytically-impaired mutant enzymes. SXA eluted towards the end of the gradient. Pooled fractions containing SXA were diafiltered against Buffer A and injected onto a Mono Q column (1.6×10 cm) equilibrated with Buffer A. The column was washed with Buffer A until absorbance at 280 nm of the eluate became minimal (~50 mL) and then developed with a 300-mL linear gradient (Buffer A to Buffer A + 1 M NaCl). Fractions (7 mL) containing SXA were pooled, frozen in liquid $N_2$ and stored at –80°C until use. The procedure produced homogeneous SXA and SXA mutant proteins by SDS-PAGE analysis. Overall purification of SXA on a protein basis was a factor of approx 3, which is consistent with approx 30% of the soluble protein in induced cells containing SXA as estimated by SDS-PAGE. Protein concentrations were estimated by using a Warburg and Christian method for impure samples and by using an extinction coefficient at 280 nm of 129600 $M^{-1}cm^{-1}$ for homogeneous SXA and SXA mutants, calculated from amino acid composition *(18)*.

### *Nuclear Magnetic Resonance Experiments*

SXA, substrates (X2 and 4NPX), and buffer (100 m*M* sodium phosphate, pH 6.0) were lyophilized, dissolved in $D_2O$, and relyophilized to convert exchangeable protons to deuterium. Buffer and substrates were redissoved in $D_2O$ and added to a 5-mm nuclear magnetic resonance (NMR) tube. After a reference spectrum of the substrate was completed, enzyme (10 μL enzyme in $D_2O$) was added to yield initial reaction conditions of 3 m*M* X2 or 4NPX, 170 n*M* enzyme, 70 m*M* sodium phosphate, pD 6.0, and 27°C. The reaction was monitored by $^1H$ NMR with a Bruker DX 500 MHz spectrometer. Time points reported represent the time when the data collection began; each time point consists of 16 scans and took approximately a minute to acquire.

### *Kinetics With 4NP Substrates*

Two methods were employed for determining initial rates. In Method A (discontinuous monitoring), aliquots (0.02–0.2 mL) were removed from temperature-equilibrated reaction mixtures at varying time points, placed into a cuvet containing 0.80–0.98 mL 0.1 *M* NaOH (or 1 *M* $Na_2CO_3$ at pH 11.0 for 4NPA) so that the final volume was 1 mL, and the absorbance was read at 410 nm. Initial rates were calculated from fitting the absorbance readings vs time to a line (minimum of 4 points per reaction progression) and by using an extinction coefficient of 17.4 $mM^{-1}cm^{-1}$. In Method B (continuous monitoring), temperature-equilibrated reactions (1 mL) were monitored at 380 nm (for pH values below 6.0) or 400 nm (for pH values of 6.0 and above). Reactions were generally monitored 0.3 min for initial rate determinations. Delta extinction coefficients (product – substrate) used for molar conversion were determined by subtracting the absorbance of substrate (at pH 5.0 so even very minor contaminating 4NP would not contribute) from the absorbance of 4NP for each reaction condition. The concentration of 4NP used for these determinations was calculated using the reported extinction coefficient of 18.3 $mM^{-1}cm^{-1}$ at 400 nm for 4NP in NaOH *(19)*. The concentration of 4NP substrates was determined by incubating the substrate with excess enzyme until an end point was reached, adding an aliquot (0.01 to 0.1 mL) to 0.1 *M* NaOH, recording the absorbance at 400 nm and using the extinction coefficient of 18.3 $cm^{-1}mM^{-1}$. Unless indicated otherwise, for both Methods A and B, reactions were initiated by adding a small aliquot of enzyme (generally, 7 μL of enzyme diluted into 10 m*M* sodium phosphate, pH 7.0, and incubated on wet ice or at ~25°C) to the 1-mL, temperature-equilibrated (25°C) reaction mixtures. For pH studies, buffers of constant ionic strength ($I$ = 0.3 *M*), adjusted with NaCl, were used as indicated: 100 m*M* succinate-NaOH (pH 4.3–6.0), 100 m*M* sodium phosphate (pH 6.0–8.0), 30 m*M* sodium pyrophosphate (pH 8.0–9.0), glycine-NaOH (pH 9.0) and glycylglycine-NaOH (pH 9.0). The parameter, $k_{cat}$, is expressed in moles of substrate hydrolyzed per s per mole of enzyme active sites (monomers), the latter calculated from the 280 nm extinction coefficient for SXA.

### Kinetics With Substrates 4NPX2, A2 and X2-X6

Products from SXA-catalyzed hydrolysis of substrates 4NPX2, A2, and X2-X6, were separated and quantified by using a DX500 HPLC system with an ED40 electrochemical detector (pulsed amperometry), AS3500 autosampler, PA-100 (4×250 mm) anion exchange column, and Chromeleon software (Dionex Corp.). Samples (25 µL) were injected onto the column equilibrated with 0.1 *M* NaOH and developed with a 15-min linear gradient (0.1 *M* NaOH to 15 m*M* sodium acetate) at approx 25°C and a flow rate of 1 mL $min^{-1}$. Several concentrations of the products of interest (e.g., D-xylose, 4NPX2, 4NPX, L-arabinose, and X2-X6) were used to establish standard curves on the same day experimental samples were run. Substrate concentrations were determined by HPLC analysis of samples incubated with excess SXA for complete conversion to D-xylose or L-arabinose.

For X2-X6 substrates, 1-mL reaction mixtures contained varied substrate concentrations (0.3–7 m*M*), 100 m*M* succinate-NaOH, pH 5.3 at 25°C. Before (time = 0 min) and after (time = 1–6 min) initiating reactions with enzyme (7 µL), samples (0.05–0.1 mL) were removed and quenched with an equal volume of 0.5 *M* acetic acid and frozen. Following lyophilization, samples were dissolved in $H_2O$ and analyzed by high-performance liquid chromatography (HPLC). Initial rates were calculated from linear regressions of the [D-xylose] produced vs time, rejecting later time points when they did not fit the line due to excess substrate consumption. The parameter, $k_{cat}$, is expressed in moles of substrate hydrolyzed per s per mole enzyme active sites (monomers); thus, for substrate X2, the product [D-xylose] produced was divided by two to provide the [X2] hydrolyzed, whereas for X3-X6, the [D-xylose] produced was taken as the concentration of substrate hydrolyzed. For progress curves of SXA-catalyzed hydrolysis of X4 and X6, reactions (2 mL) contained 100 m*M* succinate-NaOH, pH 5.3 at 25°C. Before and after addition of enzyme (7 µL), 25-µL aliquots of the reaction mixtures were directly injected onto the HPLC column for quantification of X1-X6 carbohydrates. Results from two replicate reactions were combined to provide data points for the progress curves.

In determination of initial rates for the SXA-catalyzed hydrolysis of A2, reaction mixtures (0.3 mL) contained A2 (0.2–9.0 m*M*), 100 m*M* succinate-NaOH, pH 5.3 at 25°C. Before and after addition of enzyme (7 µL), 25-µL aliquots of the reaction mixtures were directly injected onto the HPLC column for quantification of product L-arabinose. Several replicate reactions of each A2 concentration were used to generate varied time points (0–30 min) for linear regressions of product L-arabinose produced versus time. Initial rates are expressed as moles of A2 hydrolyzed per s per mole SXA active sites (monomers); thus the [L-arabinose] produced in reaction was divided by two to provide the [A2] hydrolyzed.

Reaction mixtures with varied concentrations of 4NPX2 (0.028–0.184 m*M*) contained 100 m*M* sodium phosphate, pH 7.0 at 25°C. Before (time = 0) and after (time = 1 and 2 min) initiating 0.5-mL reactions with 7 µL SXA,

0.1-mL aliquots were removed and quenched with 0.1 mL of 60 m*M* sodium pyrophosphate, pH approx 12.0 at 4°C so that the quenched sample was approx pH 10.0. Quenched samples were analyzed by HPLC for D-xylose. Initial rates were determined from linear regressions of [D-xylose] produced vs reaction time. The determined rates are expressed as moles D-xylose produced per s per mole SXA active sites. For progress curves, reaction mixtures contained 0.092 m*M* 4NPX2, 100 m*M* sodium phosphate, pH 7.0 at 25°C. Before (time = 0) and after (time = 1–20 min) initiating 1-mL reactions with 7 µL SXA, 0.2-mL aliquots were removed and quenched with 0.2 mL sodium pyrophosphate pH approx 12.0 at 4°C. Quenched samples were split: one aliquot (0.15 mL) was analyzed by HPLC for D-xylose, 4NPX2, and 4NPX; the other aliquot (0.2 mL) was analyzed for 4NP by adding it to 0.8 mL of 0.1 *M* NaOH, recording the absorbance at 400 nm and using an extinction coefficient of 18.3 $mM^{-1}cm^{-1}$ *(19)*. Four 1-mL replicate reactions were conducted to supply data points for the progress curves. Two parallel reactions were conducted, under the same conditions with the same reaction components, the absorbance at 400 nm was continuously monitored (20 min) for 4NP production, and the absorbance values were converted to mM 4NP concentrations by using a delta extinction coefficient (product – substrate) of 8.22 $mM^{-1}cm^{-1}$.

## *Equations*

Data were fitted to Eqs. 1–7 by using the computer program Grafit (Erithacus Software). Symbol definitions in order of occurrence: ν is the observed initial rate of catalysis, $k_{cat}$ is the maximum rate of catalysis, $S$ is the substrate concentration, $K_m$ is the Michaelis constant, $I$ is the inhibitor concentration, $K_i$ is the inhibitor dissociation constant, $p$ is the determined parameter at a single pH, $P$ is the pH-independent value of the parameter, $K_a$ is the acid dissociation constant of the group affecting $P$, $H^+$ is the proton concentration, $K_{a1}$ is the acid dissociation constant of the first group affecting $P$, $K_{a2}$ is the acid dissociation constant of the second group affecting $P$, $P_1$ is the lower limit of $p$ with respect to pH, $P_2$ is the upper limit of $p$ with respect to pH, and $P_3$ is the middle limit of $p$ with respect to pH.

$$v = \frac{k_{cat} * S}{K_m} \tag{1}$$

$$v = \frac{k_{cat} * S}{K_m * (1 + \frac{I}{K_1}) + S} \tag{2}$$

$$p = \frac{P}{1 + \frac{K_a}{H^+}} \tag{3}$$

$$p = \frac{P}{1 + \frac{H^+}{K_a}} \tag{4}$$

$$p = \frac{P}{1 + \frac{H^+}{K_{a1}} + \frac{K_{a2}}{H^+}} \quad (5)$$

$$p = P_1 + \frac{P_2 - P_1}{1 + \frac{H^+}{K_a}} \quad (6)$$

$$p = \frac{P_3}{1 + \frac{H^+}{K_{a1}}} + \frac{P_2 - P_3}{1 + \frac{H^+}{K_{a2}}} \quad (7)$$

## Results and Discussion

### *Models of Enzyme-Substrate Complexes*

Recently, X-ray structures of GH43 β-xylosidases have been deposited in the Protein Data Bank (PDB ID CODES, species: 1YI7, *Clostridium acetobutylicum*; 1YIF, *Bacillus subtilis*;1YRZ, *Bacillus halodurans*; 1Y7B, *Clostridium acetobutylicum*). The structures are of homotetrameric proteins with monomers containing two domains, one of which is similar to the five-bladed β propeller domain found in a GH43 arabinanase from *Cellvibrio cellulosa (20)*, which is a homodimer of monomers comprising the singe domain. Protein sequence identity of SXA against the GH43 β-xylosidases with reported X-ray structures is 53–72%, and none of the X-ray structures contain glycone ligands in the active site useful for computer docking of substrates. We chose the structure of β-xylosidase from *C. acetobutylicum* (PDB ID: 1YI7) for modeling because of its highest percentage sequence identity to SXA; as well, within a 9 Å sphere of the active site of 1YI7, all 21 residues are identical in the sequence of SXA. One X-ray structure of the GH43 arabinanase (PDB ID: 1GYE) contains 1,5-α-L-arabinohexaose (A6) in the active site of a catalytically-debilitated mutant of the enzyme. A6 was computationally transferred as a rigid body from the mutant arabinanase structure to the structure of β-xylosidase from *C. acetobutylicum* by aligning the backbones of the five-bladed β propeller domains (root mean square deviation of 812 pairs of atoms fitted = 1.4 Å), followed by aligning two atoms of the catalytic acid and one atom of the catalytic base for a minor adjustment. The resulting model of xylosidase complexed with A6 indicates that two residues of the nonreducing end of the oligosaccharide are in steric conflict with the xylosidase protein: subsites –3, and –2 of the arabinanase are blocked by protein in the xylosidase (Fig. 1); note that subsite –1 refers to the protein site that binds the first residue on the nonreducing side of the glycosidic bond of substrate that is cleaved and more negative numbering indicates subsites that are further removed from the cleaved bond on the nonreducing side; subsite +1 refers to the protein site that binds the first residue on the reducing side of the cleaved bond and more positive numbering indicates subsites that are further removed from

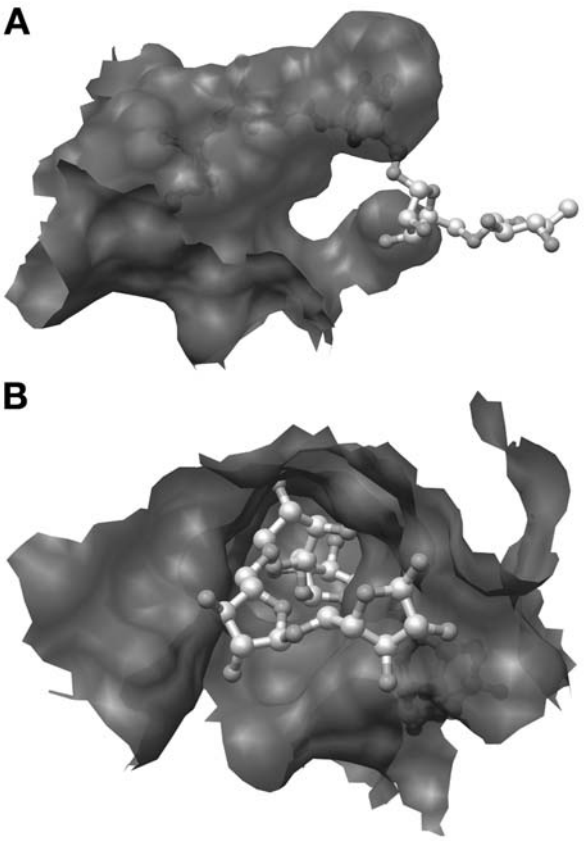


Fig. 1. Molecular surface model of the SXA active site with docked 1,5-α-L-arabinohexaose. The model is based on the X-ray structures of β-xylosidase (PDB ID: 1YI7) and arabinanase with arabinohexaose bound (PDB ID: 1GYE), both enzymes of GH43. **(A)** View indicating that two residues of the nonreducing end of the arabinohexaose are excluded from the SXA active-site pocket. The arabinanase used for the model cleaves the arabinohexaose to yield two equivalents of arabinotriose. Because the general acid and general base of the arabinanase are aligned with those of the xylosidase, the exclusion of two residues of the nonreducing end of the arabinohexaose suggests that SXA cleaves a single residue from the nonreducing end of substrate. **(B)** View showing four residues of the arabinohexaose extending from the opening of the active-site pocket. Note that two arabinose residues of the reducing end of arabinohexaose protrude from the SXA active site with few protein interactions.

the cleaved bond on the reducing side *(21)*. Blockage of subsites –3 and –2 is conferred primarily by the presence of F507 and F508 (SXA residue numbering is used throughout the work; it differs from that of the *C. acetobutylicum* β-xylosidase by 1–6) of the xylosidase C terminus within the same subunit as the active site that is blocked. There are no corresponding residues in the arabinanase as its C terminus ends at residue 346. The arabinanase cleaves A6 to two equivalents of arabinotriose, but the model of Fig. 1 suggests that the xylosidase, having a shallower active-site cavity, cleaves a single monosaccharide from the nonreducing end.

1,5-α-L-Arabinobiose (A2) is accepted as a substrate by SXA (*see* "Natural Substrates"). A model of A2 in the xylosidase active site was built by clipping two arabinose residues from the nonreducing end and two residues from the reducing end of A6 in the model of Fig. 1 (Figs. 2A and 3). In the model, the carboxylate oxygen of D14 is approx 6 Å from the anomeric carbon of the scissile bond and the carboxylate oxygen of E186 is approx 4 Å from the glycosidic oxygen atom of substrate. The distances are similar to those found in other glycoside hydrolases that act by inverting the configuration of the anomeric carbon of substrate: thus, in Fig. 2 there is space to accommodate a water molecule between the carboxyl group of D14 and the anomeric carbon of substrate for addition and the carboxyl group of E186 is in position to protonate the oxygen atom bridging arabinose residues. The carboxyl group of D14 shares a salt bridge with the guanidinium group R290 and an H bond with the imidazole group of H248. The carboxyl group of E186 shares an H bond with the carboxyl group of D127. Together, E186, D127, H248, D14 and R290 form an H bonding network within subsite –1.

Xylobiose (X2) was built into the model of xylosidase using the A2 ligand as a guide, overlaying atoms of the glycosidic bond that is cleaved and the C3 of the reducing xylose onto the C2 of the reducing arabinose residue of A2 to generate the model (Fig. 2B). Similarly to the model with A2 in the active site, X2 is well positioned to serve as substrate (with similar distances reported for the SXA-A2 model). X2 is an excellent substrate for SXA (*see* "Natural Substrates").

D-Xylose, substituted at the 2′ or 3′ OH group with L-arabinofuranose, is a constituent of xylan from certain plant species and a potential substrate for SXA and other β-xylosidases. 1,3-α-Arabinofurano-D-xylose (AX) was built into the active-site model of SXA by replacing the arabinose residue of the reducing end of A2 (in the model of Fig. 2A) with D-xylose (Fig. 2C). The model suggests that AX is in a good position to serve as substrate. As well, it suggests that the arabinose substitutions of xylooligosaccharides must be to the nonreducing end of the chain for SXA to catalyze its cleavage; i.e., the arabinofuranose residue must occupy subsite –1 of SXA. Moreover, if there is more than one arabinose substitution to a xylooligosaccharide, it could not be accommodated by subsite +1 and would have to be two or three residues more towards the reducing end of the xylooligosaccharide, which extend to bulk solvent. AX, specifically, has not been studied as a substrate for SXA, but SXA has been shown to liberate arabinose residues from arabinoxylan, digested to oligosaccharides by xylanase *(12)*. Coordinates of the models shown in Figs. 1–3 are available from the corresponding author.

### $^1$H NMR Determination of Reaction Stereochemistry

GH43 is annotated to catalyze hydrolysis of substrates to products through inversion of stereochemistry of the anomeric carbon (http://afmb.cnrs-mrs.fr/CAZY). The inversion mechanism has been determined

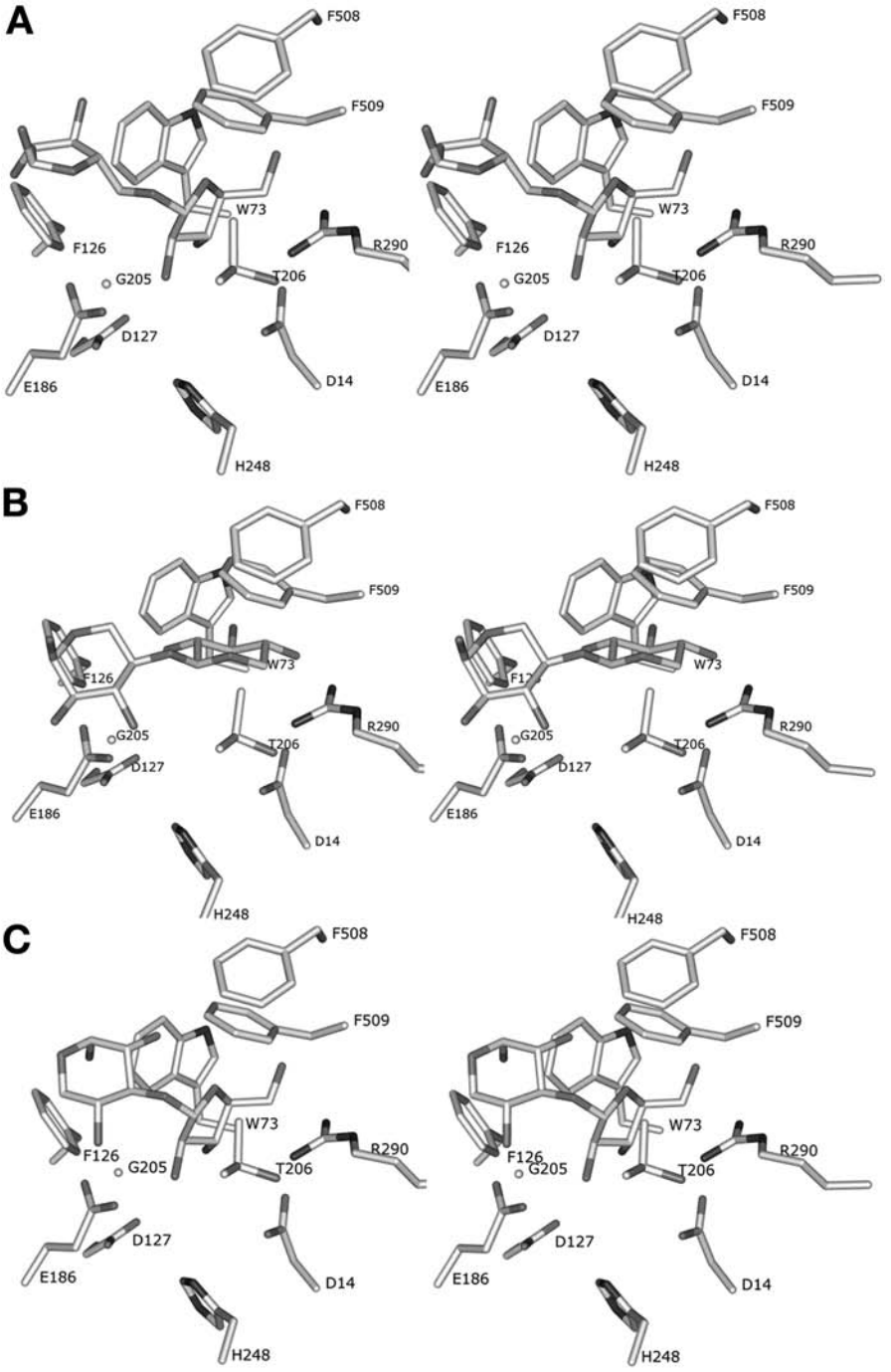


Fig. 2. Models of disaccharide substrates docked in the active site of SXA. Stereo views are of a sphere emanating 6 Å from the oxygen atom bridging the two monosaccharide residues. Key residues, D14, D127 and H248, which are approx 1 Å outside the 6 Å radius, are added to the view. **(A)** 1,5-α-L-Arabinobiose (A2). **(B)** 1,4-β-D-Xylobiose (X2). **(C)** α-Arabinofurano-D-xylose (AX).

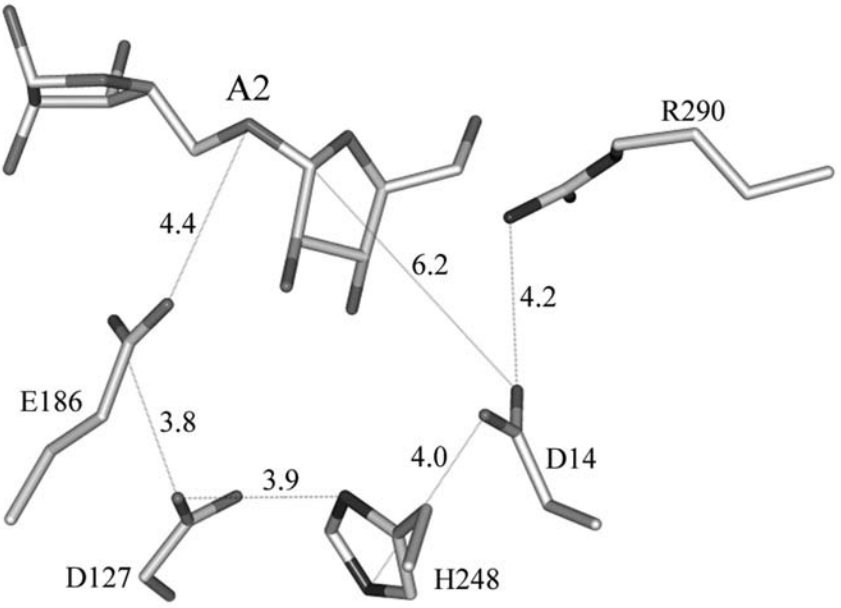


Fig. 3. Model of 1,5-α-L-arabinobiose (A2) docked in the active site of SXA. Key residues and distances (in Å) are shown.

experimentally for a GH43 β-xylosidase from *Bacillus pumilus* acting on substrate 4NPX and using an enzyme coupling reaction that specifically reports for α-xylose *(22)* and for a GH43 β-xylosidase from *Butyrivibrio fibrisolvens* acting on 2-nitrophenyl-β-D-xylopyranoside by using an HPLC separation method *(23)*. Stereochemistry of GH43 xylosidases acting on xylooligosaccharides has not been reported. We used $^{1}$H NMR to determine the stereochemistry of 4NPX and X2 hydrolysis reactions catalyzed by SXA (Fig. 4). For 4NPX, the enzymatic reaction was complete in approx 5 min. At 4 min, the anomeric isomer ratio (α:β) in the D-xylose product was 20:1. That 100% of the D-xylose product was not found in the α configuration is likely due to mutarotation from α to β, which has a half-life of <1 h under the incubation conditions. After incubation 24 h, the anomeric isomer ratio at equilibrium was determined as 1:2.5. For substrate X2, the enzymatic reaction was faster and the reaction had reached completion at the first time point (45 s) after enzyme addition. At 45 s, the anomeric isomer ratio (α:β) of the xylose product was 6:1. The 6:1 ratio suggests that the anomeric carbon of X2, not sharing the scissile bond, has an isomeric ratio (α:β) of 2.5:1. After incubation 24 h, the anomeric isomer ratio at equilibrium was determined as 1:2.5. Thus, SXA catalyzes the hydrolysis of 4NPX and X2 by inversion of configuration of the anomeric carbon sharing the scissile bond. This invokes a single step mechanism (single transition state) for the hydrolysis reactions catalyzed by SXA.

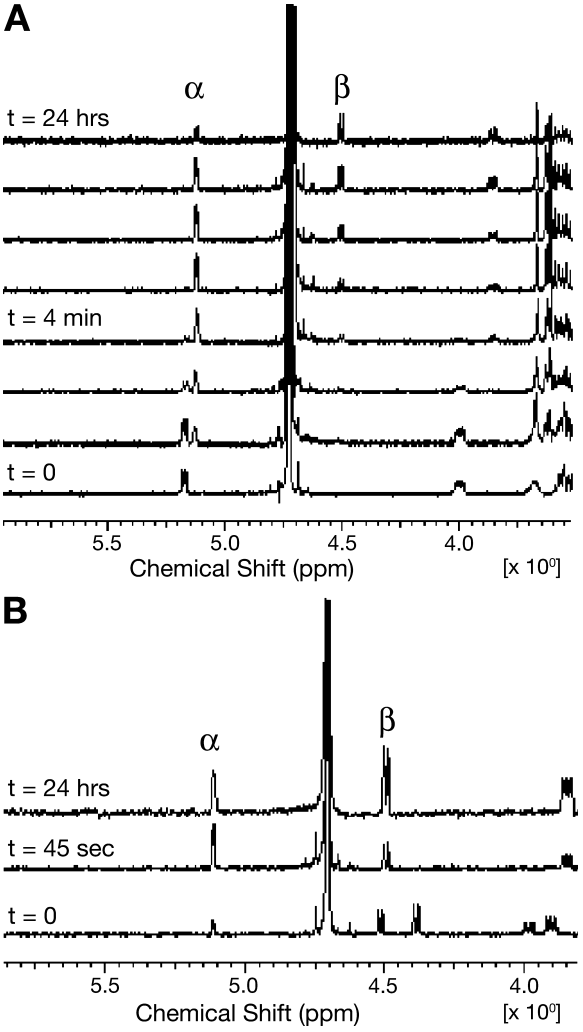


Fig. 4. $^{1}$H nuclear magnetic resonance monitoring of SXA-catalyzed hydrolysis of 4-nitrophenol-β-D-xylose (4NPX) and 1,4-β-xylobiose (X2). **(A)** 4NPX. The bottom spectrum is a reference spectrum of 4NPX before enzyme addition (time = 0). After the addition of enzyme the spectra, in ascending order, are time = 45 s, 2.5 min, 4 min, 5.5 min, 7 min, 11 min, and 24 h. **(B)** X2. The bottom spectrum is a reference spectrum of X2 before enzyme addition (time = 0). After the addition of enzyme the spectra, in ascending order, are time = 45 s and 24 h.

## *4NP-Glycoside Substrates*

For experimental convenience and latitude, it is desirable to have the availability of several 4NP-glycosides as substrates for the study of SXA. A survey of commercially available 4NP-gylcosides found that only two (4NPX and 4NPA) serve as substrates for the enzyme (Table 2). Upon first inspection, 4-nitrophenyl-β-L-arabinopyranoside appeared to serve as a substrate, having a rate less than 0.1% that of 4NPX under the reaction

Table 2
Survey of 4NP-Glycosides as Potential Substrates of SXA[a]

| 4NP-Glycoside (5 m*M*) | Relative rate[b] |
|---|---|
| 4-Nitrophenyl-β-D-xylopyranoside (4NPX) | 1.00 ± 0.01 |
| 4-Nitrophenyl-α-L-arabinofuranoside (4NPA) | 0.101 ± 0.003 |
| 4-Nitrophenyl-β-L-arabinopyranoside[c] | $<10^{-6}$ |
| 4-Nitrophenyl-α-L-fucopyranoside | $<10^{-6}$ |
| 4-Nitrophenyl-β-L-arabinopyranoside | $<10^{-6}$ |
| 4-Nitrophenyl-β-D-glucopyranoside | $<10^{-6}$ |
| 4-Nitrophenyl-β-D-mannopyranoside | $<10^{-6}$ |
| 4-Nitrophenyl-α-D-xylopyranoside | $<10^{-6}$ |
| 4-Nitrophenyl-β-D-fucopyranoside | $<10^{-6}$ |
| 4-Nitrophenyl-α-D-galactopyranoside | $<10^{-6}$ |
| 4-Nitrophenyl-β-D-galactopyranoside | $<10^{-6}$ |
| 4-Nitrophenyl-α-D-mannopyranoside | $<10^{-6}$ |
| 4-Nitrophenyl-α D-glucopyranoside | $<10^{-6}$ |
| 4-Nitrophenyl-α-L-rhamnopyranoside | $<10^{-6}$ |
| 4-Nitrophenyl-β-L-fucopyranoside | $<10^{-6}$ |

[a]Reactions contained 5 m*M* 4NP glycoside in 100 m*M* succinate-NaOH, pH 5.3 and 25°C. Initial rates were determined by using Method A.

[b]Initial rates are expressed as relative to that of 4NPX (25.1 $s^{-1}$). Standard deviations of replicates are indicated. Limit of detection $<10^{-6}$, estimated from having 1.2–2.4 × $10^3$-fold larger enzyme concentrations, (7.7–15.4 μ*M*), 100-fold longer reaction times, and the ability to detect 10-fold smaller changes in absorbance per min in comparison to 4NPX reactions.

[c]This glycoside was contaminated with a small percentage (0.08%) of a 4NP substrate that was hydrolyzed by SXA. To determine substrate activity for the remaining 99.9%, samples were incubated with a high concentration of SXA (7.7 μ*M*) to consume the impurity and the hydrolysis rate was determined from the reaction progression that followed.

conditions shown in Table 2. Further examination of the potential substrate, monitoring its progression to 4NP in a reaction catalyzed by SXA, indicated that only 0.08% of the 4NP-glycoside can be hydrolyzed by SXA. After incubating SXA for 1 h in the absence or presence of the preparation of 4-nitrophenyl-β-L-arabinopyranoside, aliquots were removed and assayed with substrate 4NPX; enzyme incubated in the absence or presence of the preparation had the same catalytic activity, indicating that SXA was not inactivated by the preparation. Therefore, 99.9% of the 4-nitrophenyl-β-L-arabinopyranoside preparation does not serve as a substrate for SXA, and it is likely that the commercial preparation was contaminated with a 4NP-glycoside that serves as a substrate (possibly 4NPA).

Steady-state kinetic parameters of SXA-catalyzed hydrolysis of 4NPX or 4NPA were modestly influenced by increased viscosity (Table 3). When 50% sucrose was included in the reaction mixtures, $k_{cat}$ and $k_{cat}/K_m$ for substrates 4NPX and 4NPA were eroded by less than 12%, indicating that diffusion is a minor kinetic factor limiting SXA-catalyzed hydrolysis of

Table 3
Influence of Viscosity on SXA Steady-State Kinetic Parameters[a]

| Substrate/exper. no. | $\eta/\eta_o$[b] | $k_{cat}$($s^{-1}$) | $k_{cat}$ Rel. to $\eta/\eta_o = 1$ | $k_{cat}/K_m$ ($s^{-1}mM^{-1}$) | $k_{cat}/K_m$ Rel. to $\eta/\eta_o = 1$ | $K_m$ (m*M*) |
|---|---|---|---|---|---|---|
| 4NPX/1[c] | 1.00 | 32.8 ± 0.6 | 1.00 | 44.1 ± 2.4 | 1.00 | 0.742 ± 0.041 |
| 4NPX/1[c] | 6.12 | 29.8 ± 0.5 | 0.910 ± 0.0152 | 43.1 ± 2.2 | 0.980 ± 0.050 | 0.690 ± 0.035 |
| 4NPX/2[d] | 1.00 | 32.9 ± 0.5 | 1.00 | 47.1 ± 1.7 | 1.00 | 0.699 ± 0.035 |
| 4NPX/2[d] | 6.85 | 30.1 ± 1.1 | 0.920 ± 0.040 | 41.6 ± 3.5 | 0.880 ± 0.080 | 0.637 ± 0.081 |
| 4NPA/2[d] | 1.00 | 2.99 ± 0.05 | 1.00 | 4.01 ± 0.14 | 1.00 | 0.745 ± 0.036 |
| 4NPA/2[d] | 6.85 | 2.87 ± 0.12 | 0.960 ± 0.040 | 3.81 ± 0.37 | 0.950 ± 0.100 | 0.754 ± 0.101 |

[a]Viscosity was varied by the absence or presence of 50% (wt/vol) sucrose in the reaction mixtures. Initial-rate data were fitted to Eq. 1 for determination of kinetic parameters. Standard errors are indicated.

[b]Viscosity of reaction solution relative to that of water.

[c]Reactions contained variable concentrations of 4NPX in 100 m*M* succinate-NaOH, pH 5.3 at 25°C. Initial rates were determined by Method A.

[d]Reactions contained variable concentrations of 4NPX or 4NPA in 100 m*M* MES-NaOH, pH 6.00 at 25°C. Initial rates were determined by Method B.

these substrates. Had the reactions been fully controlled by diffusion, the kinetic parameters would be degraded by more than 80%.

Stopped-flow experiments, recording reactions (at 400 nm) of 4 m*M* 4NPX or 4NPA with 10 μ*M* SXA in 100 m*M* sodium phosphate, pH 7.0, $I = 0.3$ *M* and 25 °C, gave no indication of bursts (or lags) in the production of 4NP, ruling out the possibility of slow release of products limiting the steady-state rates for these substrates. Moreover, zero-order rates, determined by using the stopped-flow in 100 ms reactions, were similar (within 5%) to the zero-order rates determined by using the conventional spectrophotometer in 30 min reactions under the same buffer, temperature and substrate conditions but much lower concentration of SXA.

A recent study of the GH43 β-xylosidase from *Geobacillus stearothermophilus* reported that the progress curve of the enzyme-catalyzed hydrolysis of 4-nitrophenyl-β-D-xylobioside (4NPX2) shows a lag in 4NP production *(6)*, suggesting that the enzyme catalyzes hydrolysis of the D-xylose residue occupying the nonreducing end of 4NPX2 (to yield D-xylose and 4NPX) instead of catalyzing hydrolysis of the 4NP residue from the opposite end of 4NPX2. However, production of D-xylose and 4NPX and consumption of 4NPX2 were not monitored quantitatively, leaving the possibility that all products and substrates display lags. We monitored progress of SXA-catalyzed hydrolysis of 4NPX2 using HPLC and spectrophotometric methods for determining the concentrations of 4NPX2, 4NPX, D-xylose, X2 and 4NP (Fig. 5). The progress curves indicate that there is a lag in the production of 4NP, but not in the production of D-xylose or 4NPX and not in the consumption of 4NPX2, ruling out the possibility that the lag in 4NP production owes to hystereses of SXA action on 4NPX2. There was no accumulation of X2. It strongly suggests that SXA catalyzes the hydrolysis of 4NPX2 in two steps without processivity: in the first, d-xylose is cleaved from the nonreducing end of 4NPX2 and products D-xylose and 4NPX leave the enzyme; and, in the second, D-xylose is cleaved from the nonreducing end of 4NPX. Kinetic parameters for first step of SXA-catalyzed hydrolysis of 4NPX2 (4NPX2 to 4NPX + d-xylose) were determined (in the same reaction buffer) by HPLC analyses of product D-xylose: $k_{cat} = 50.5 \pm 25.7\ s^{-1}$, $k_{cat}/K_m = 73.3 \pm 8.4\ s^{-1}mM^{-1}$, and $K_m = 0.69 \pm 0.43$ m*M*. Kinetic parameters for the second step (4NPX to 4NP + D-xylose) were determined (in the same reaction buffer) spectrophotometrically (Method B): $k_{cat} = 16.2 \pm 0.09\ s^{-1}$, $k_{cat}/K_m = 36.6 \pm 0.5\ s^{-1}mM^{-1}$, and $K_m = 0.443 \pm 0.008$ m*M*. The kinetic parameters and concentrations of SXA (24.8 nM) and 4NPX2 (0.092 m*M*) were used as inputs for KINSIM calculations to a model that assumes rapid equilibrium binding, a single residue from the nonreducing end of substrate is cleaved per catalytic cycle and lack of processivity so that hydrolysis products are removed from SXA at the end of each catalytic cycle prior to initiating a new one. The simulation closely fits the observed concentrations of 4NPX2, D-xylose, 4NPX and 4NP in the progress curves of Fig. 5, thus reinforcing the conclusion that SXA catalyzes the hydrolysis of 4NPX2 in two steps by removing a D-xylose residue from the nonreducing end of

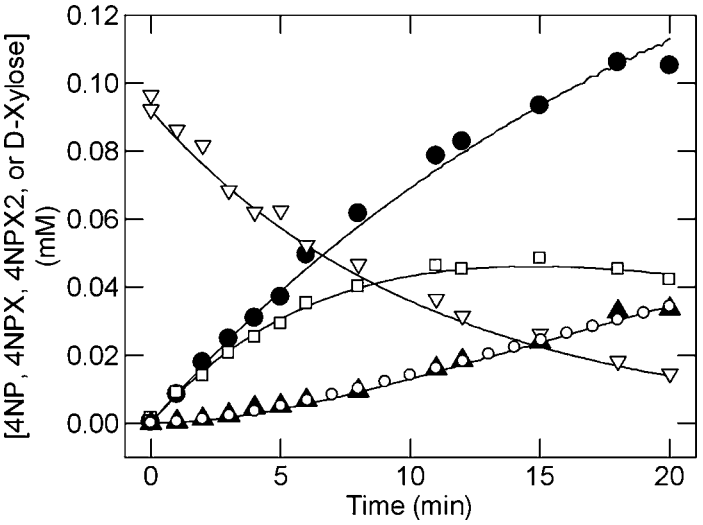


Fig. 5. Progress curves for SXA-catalyzed hydrolysis of 4NPX2. Reactions contained 24.8 n*M* SXA, 0.092 m*M* 4NPX2, 100 mM sodium phosphate, pH 7.0 and 25°C. Before and after enzyme addition, aliquots were removed with time, quenched and analyzed for substrate and product concentrations: 4NPX2 (▽), 4NPX (□), 4NP (▲), D-xylose (●). In a parallel reaction the absorbance at 400 mm was continuously monitored for a second determination of [4NP] (○). Curves were generated from a KINSIM calculation, using the indicated concentrations of SXA and 4NPX2 and kinetic parameters for SXA acting on 4NPX2 and 4NPX (determined using the same buffer and temperature conditions) as inputs in the following kinetic scheme: E + 4NPX2 ↔ E4NPX2 ($K_m$ = 0.69 ± 0.43 m*M*); E4NPX2 → E + 4NPX + X1 ($k_{cat}$ = 50.5 ± 25.7 $s^{-1}$); E + 4NPX ↔ E4NPX ($K_m$ = 0.443 ± 0.008 mM); E4NPX → E + 4NP + X1 ($k_{cat}$ = 16.2 ± 0.09 $s^{-1}$). The KINSIM model assumes rapid equilibrium binding, a single D-xylose is hydrolyzed from the nonreducing end of substrate per catalytic cycle and lack of processivity.

substrate in each step without processivity. It should be noted that, whereas $k_{cat}$(4NPX2) and $K_m$ (4NPX2) are not well determined because the highest substrate concentration was well below the $K_m$ in the determination, $k_{cat}/K_m$(4NPX2) is fairly well determined and the latter parameter was most important in the KINSIM calculations of the reaction progress that was conducted under $k_{cat}/K_m$ conditions.

## *Site-Directed Mutations and Catalysis*

According to the models of Fig. 2, D14 is positioned to serve as a general base activating a water molecule for addition to the anomeric carbon of substrate and E186 is positioned to protonate the leaving group oxygen atom. Residues D128, H248 and R290 form an H bonding network with D14 and E186, likely for the purpose of positioning the side chains of D14 and E186 for reacting with substrate and to manipulate their p$K_a$ values for reactivity. Individual mutation of the residues to alanine degrades $k_{cat}$(4NPX) by factors of 3300, 12000, 24000, 330, and 2500 for D14A, E186A,

Table 4
Effect of Site-Directed Mutations of SXA
on Steady-State Kinetic Parameters With Substrate 4NPX[a]

| SXA | $k_{cat}$ ($s^{-1}$) | $k_{cat}/K_m$ ($s^{-1}mM^{-1}$) | $K_m$ (m*M*) |
|---|---|---|---|
| Wild-type | 31.1 ± 0.4 | 40.7 ± 1.6 | 0.763 ± 0.031 |
| D14A | 0.00954 ± 0.00016 | 0.0123 ± 0.0006 | 0.777 ± 0.036 |
| E186A | 0.00267 ± 0.00005 | 0.00242 ± 0.00012 | 1.10 ± 0.05 |
| D127A | 0.000129 ± 0.000003 | 0.000150 ± 0.000010 | 0.881 ± 0.059 |
| H248A | 0.0950 ± 0.0025 | 0.0909 ± 0.0063 | 1.05 ± 0.07 |
| R290A[b] | 0.0126 ± 0.0020 | 0.000250 ± 0.000044 | 50.3 ± 8.8 |

[a]Reactions contained varied concentrations of 4NPX in 100 m*M* succinate-NaOH, pH 5.3 and 25°C. Initial rates, determined by using Method A, were fitted to Eq. 1 for determination of kinetic parameters. Standard errors are indicated.

[b]Values of $k_{cat}$ and $K_m$ were not well determined for R290A because the highest concentration of 4NPX examined (5 m*M*) is far below the estimated $K_m$.

D127A, H248A, and R290A, respectively, confirming the individual importance of the native residues to catalysis (Table 4). $K_m$(4NPX) values were similar to wild-type with the exception of R290A, whose $K_m$(4NPX) is increased by 70-fold. Thus, four of the residues appear to exclusively serve in roles of general acid or general base (D14 and E186) or indirectly in supporting the general acid or general base (D127 and H248). R290, in addition to its role in assisting D14 in its role as a general base in the hydrolysis reaction, appears to serve as a recognition element for the substrate. The guanidinium group of R290 resides near the nonreducing end of substrate in the models of Fig. 2.

SXA mutations, D14A and E186A, degraded catalysis with substrate 4NPA to a similar extent as with substrate 4NPX (Table 5). As with substrate 4NPX, $K_m$(4NPA) values were similar to native SXA, while the $k_{cat}$ parameter was degraded by factors of 3000 and 11000 for mutations D14A and E186, respectively. Despite such drastic erosion of catalytic power in the mutants, native SXA and the mutants share similar values for relative substrate specificity for 4NPX and 4NPA: $k_{cat}/K_m$(4NPX)/$k_{cat}/K_m$(4NPA) values calculated from the values in Tables 4 and 5 are 12.3 ± 0.9, 10.2 ± 0.7, and 13.4 ± 1.3 for native SXA, D14A, and E186A, respectively. The relative substrate specificity values substantiate that substrates 4NPX and 4NPA share the same active site.

## *Natural Substrates of SXA*

By using HPLC analysis for quantification of reaction products, steady-state kinetic parameters of SXA-catalyzed hydrolysis of substrates X2-X6 and A2 were determined (Table 6). X2 is the best substrate having a $k_{cat}/K_m$ value of 99 $s^{-1}mM^{-1}$, whereas $k_{cat}/K_m$ values of approx 40 $s^{-1}mM^{-1}$ were determined for substrates X3-X6. A $k_{cat}$ of 412 $s^{-1}$ was determined for

Table 5
Effect of Site-Directed Mutations of SXA
on Steady-State Kinetic Parameters With Substrate 4NPA[a]

| SXA | $k_{cat}$ ($s^{-1}$) | $k_{cat}/K_m$ ($s^{-1}mM^{-1}$) | $K_m$ (m*M*) |
|---|---|---|---|
| Wild-type | 2.68 ± 0.06 | 3.30 ± 0.20 | 0.810 ± 0.050 |
| D14A | 0.000936 ± 0.000012 | 0.00121 ± 0.00005 | 0.771 ± 0.029 |
| E186A | 0.000239 ± 0.000008 | 0.000180 ± 0.000015 | 1.32 ± 0.11 |

[a]Reactions contained varied concentrations of 4NPA in 100 m*M* succinate-NaOH, pH 5.3 and 25°C. Initial rates, determined by using Method A, were fitted to Eq. 1 for determination of kinetic parameters. Standard errors are indicated.

Table 6
Steady-State Kinetic Parameters
of SXA Acting on Natural Substrates[a]

| Substrate | $k_{cat}$ ($s^{-1}$) | $k_{cat}/K_m$ ($s^{-1}mM^{-1}$) | $K_m$ (m*M*) |
|---|---|---|---|
| X2 | 412 ± 18 | 99 ± 8 | 4.2 ± 0.5 |
| X3 | 172 ± 14 | 45 ± 4 | 3.8 ± 0.6 |
| X4 | 150 ± 5 | 38 ± 1 | 4.0 ± 0.3 |
| X5 | 150 ± 15 | 41 ± 3 | 3.7 ± 0.6 |
| X6 | 96 ± 7 | 35 ± 4 | 2.7 ± 0.5 |
| A2 | 0.074 ± 0.003 | 0.062 ± 0.005 | 1.2 ± 0.1 |

[a]Reactions contained variable concentrations of substrate in 100 m*M* succinate-NaOH, pH 5.3 at 25°C. Initial-rate data were fitted to Eq. 1. Standard errors are indicated.

X2, which is 2-4 fold that of substrates X3-X6. Clearly, chain lengths beyond two xylose residues do not increase substrate specificity, and this corresponds with the lack of well-defined subsites beyond +1 in SXA active-site models for recognition of additional xylose residues on the reducing side of substrate. The observed decrease in $k_{cat}/K_m$ and $k_{cat}$ for X3-X6 may owe to somewhat lower flexibility of the residue occupying the +1 position that could impede deformation of substrate by enzyme in approaching the structure in the transition state. In comparison with substrate 4NPX under the same reaction conditions (Table 4), $k_{cat}$ and $k_{cat}/K_m$ for X2 are respectively 12-fold and 2-fold larger, even though 4NPX has a much better leaving group in 4NP and the noncatalyzed rate of hydrolysis of 4NPX exceeds $10^7$-fold that of X2. Hence, subsite +1 can exert considerable influence on the rate of catalysis, and thus substrate specificity. Besides SXA, there are only a few β-xylosidases for comparing kinetic parameters for xylooligosaccharides *(24–26)*. The best catalyst among these, the enzyme from *B. pumilus*, has reported $k_{cat}$ and $k_{cat}/K_m$ values for X2 of 18 $s^{-1}$ and 6.2 $s^{-1}mM^{-1}$ at pH 7.0 (the pH optimum for the catalyzed hydrolysis of 4NPX by the enzyme) and

25°C *(24)*, values that are less than 7% those of SXA. Similarly, the reported $k_{cat}$ and $k_{cat}/K_m$ values for the *B. pumilus* enzyme acting on substrates X3-X6 are less than 6% those of SXA. Assuming the noncatalyzed rate of hydrolysis for X2 is similar to that of α-methylglucopyranoside *(27)*, SXA enhances the rate of X2 hydrolysis by a factor exceeding $10^{17}$ and the dissociation constant for the transition state ($ES^{‡}$) is approx $10^{-19}$. A2 was the worst naturally-occurring substrate examined, having $k_{cat}$ and $k_{cat}/K_m$ values reduced by factors of 36 and 53, respectively, in comparison to 4NPA, and by factors of 5600 and 1600, respectively, in comparison to X2. Clearly, SXA does not accommodate well the arabinofuranose residue in subsite +1 with an α-1,5 linkage to the arabinofuranose residue in subsite –1, and it is likely that A2 does not serve as a natural substrate for SXA. In contrast, AX, with an arabinofuranose residue occupying subsite –1 and a xylose residue, subsite +1, is considered a likely natural substrate for SXA, though kinetic parameters are not yet available for AX to judge how well it is accepted by SXA.

Progress curves for SXA-catalyzed hydrolysis of X6 and X4 were monitored by using HPLC analysis for quantification of substrates and products and compared with progress curves predicted by KINSIM calculations with inputs of the kinetic parameters of Table 6 and $K_i$(xylose) = 7.4 m*M* (determined using substrate 4NPX in the same buffer at pH 5.3 at 25°C) and assuming that a single xylose residue is removed from the nonreducing end of substrate per catalytic cycle without processivity (Fig. 6). The KINSIM calculations of temporal concentrations of hydrolysis products of substrates X6 and X4 approximate the observed concentrations in the SXA-catalyzed reactions. In the hydrolysis of X6, peak heights of intermediate products (observed: KINSIM predicted) occur in the reaction coordinate as follows (values in s): X5 (3138:3140), X4 (8260:7070), X3 (10822:10750), and X2 (13384:13700). Thus, experimental data indicate temporal peaks of intermediates occur in descending order of appearance X5 > X4 > X3 > X2, which was assumed in the simulation. Similarly, in the hydrolysis of X4, the occurrence of peak heights of intermediate products (observed: KINSIM predicted) are as follows: X3 (4130:5100) and X2 (2940:3300), indicating that X3 precedes X2 as a product in the reaction coordinate. Thus, SXA-catalyzed hydrolysis of naturally-occurring substrates, X6 and X4, proceeds with a single residue cleaved per catalytic cycle in the absence of processivity

## *Influence of pH on Catalysis*

Steady-state kinetic parameters were determined at varying pH and constant ionic strength for substrates 4NPX and 4NPA (Figs. 7 and 8). SXA is unstable at pH values below 4.1, limiting the study to higher pH's. Curves for the two substrates are similar in shape for $k_{cat}/K_m$ with $pK_{a1}$ and $pK_{a2}$ values of 5.0 and 7.2 for the acidic and basic limbs, respectively: $pK_{a1} = 5.0$ for the catalytic base (D14) and $pK_{a2} = 7.2$ for the catalytic acid (E186). Thus, for substrates 4NPX and 4NPA, the pH-independent $k_{cat}/K_m$ reflects the "monoanionic" form of SXA ($D14^{-}$ $E186^{H}$), and $k_{cat}/K_m$ is fully degraded

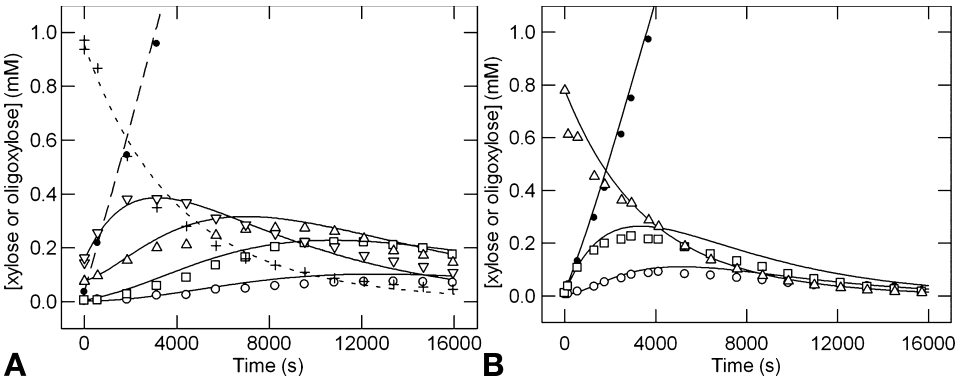


Fig. 6. Progress curves for SXA-catalyzed hydrolysis of X6 and X4. Reactions were in 100 mM succinate-NaOH, pH 5.30 and 25°C. Before and after enzyme addition, aliquots were removed with time for determination of reactant and product concentrations by high-performance liquid chromatography analysis: X1 (●), X2 (○), X3 (□), X4 (△), X5 (▽), X6 (+). Curves were generated from KINSIM calculations using the indicated concentrations of SXA and X1-X6, the kinetic parameters reported in Table 6 for X2-X6, and $K_i$(xylose) = 7.40 m*M* for inputs in the following kinetic scheme: E + X6 ↔ EX6 ($K_m$ = 2.7 m*M*); EX6 → E + X5 + X1 ($k_{cat}$ = 96 $s^{-1}$); E + X5 ↔ EX5 ($K_m$ = 3.7 m*M*); EX5 → E+ X4 + X1 ($k_{cat}$ = 150 $s^{-1}$); E + X4 ↔ EX4 ($K_m$ = 4.0 m*M*); EX4 → E + X3 + X1 ($k_{cat}$ = 150 $s^{-1}$); E + X3 ↔ EX3 ($K_m$ = 3.8 m*M*); EX3 → E + X2 + X1 ($k_{cat}$ = 172 $s^{-1}$); E + X2 ↔ EX2 ($K_m$ = 4.2 m*M*); EX2 → E + X1 + X1 ($k_{cat}$ = 412 $s^{-1}$); E +X1 ↔ EX1 ($K_i$(xylose) = 7.40 m*M*). The KINSIM model assumes rapid equilibrium binding, a single D-xylose is hydrolyzed from the nonreducing end of substrate per catalytic cycle and lack of processivity. **(A)** Reactions were initiated with enzyme to give initial concentrations of 10 n*M* SXA, 0.953 m*M* X6, 0.15 m*M* X5, 0.077 m*M* X4, 0.0042 m*M* X3, 0.0023 m*M* X2, and 0.036 m*M* X1. **(B)** Reactions were initiated with enzyme to give initial concentrations of 9.0 n*M* SXA, 0.78 m*M* X4, 0.011 m*M* X3, 0.0058 X2, and 0.016 m*M* X1.

when the enzyme becomes protonated to the "diprotic" SXA ($D14^H$ $E186^H$) or deprotonated to the "dianionic" SXA ($D14^-$ $E186^-$). The p$K_a$ values for active-site carboxylic acid residues (D14, D127, and E186) are likely raised by their proximity to one another (within 6 Å); p$K_{a1}$ = 5.0, reporting for the carboxylic group of D14, is likely made more normal by its close proximity (4.2 Å) to the guanidinium group of R290 and p$K_{a2}$ = 7.2, reporting for the carboxylic group of E186, is likely made more basic by its close proximity (3.8 Å) to the carboxylic group of D127. Curves for the two substrates differ in shape for $k_{cat}$: substrate 4NPA is mainly flat over the pH range examined and $k_{cat}$ drops on the acid side with a single p$K_a$ value of 3.6; $k_{cat}$ for substrate 4NPX shows a p$K_{a1}$ of 3.5 for a drop on the acid side and a p$K_{a2}$ of 6.9 for a drop on the basic side. The p$K_a$ values of approx 3.5 are not well determined because the lowest pH in the studies was 4.3; yet, for substrate 4NPX, omitting the $K_{a1}$ parameter of Eq. 5 (to give Eq. 3) is not preferred statistically over its inclusion (F test probability of 8%), and for substrate 4NPA, omitting the $K_a$ term of Eq. 4 (to give a line of slope = 0) is not preferred over its inclusion (F test probability of 1%). Extension by 1.5 pH units of the p$K_a$ for $k_{cat}$ over that of $k_{cat}/K_m$ would not be unusual (*28*). It is plausible that the

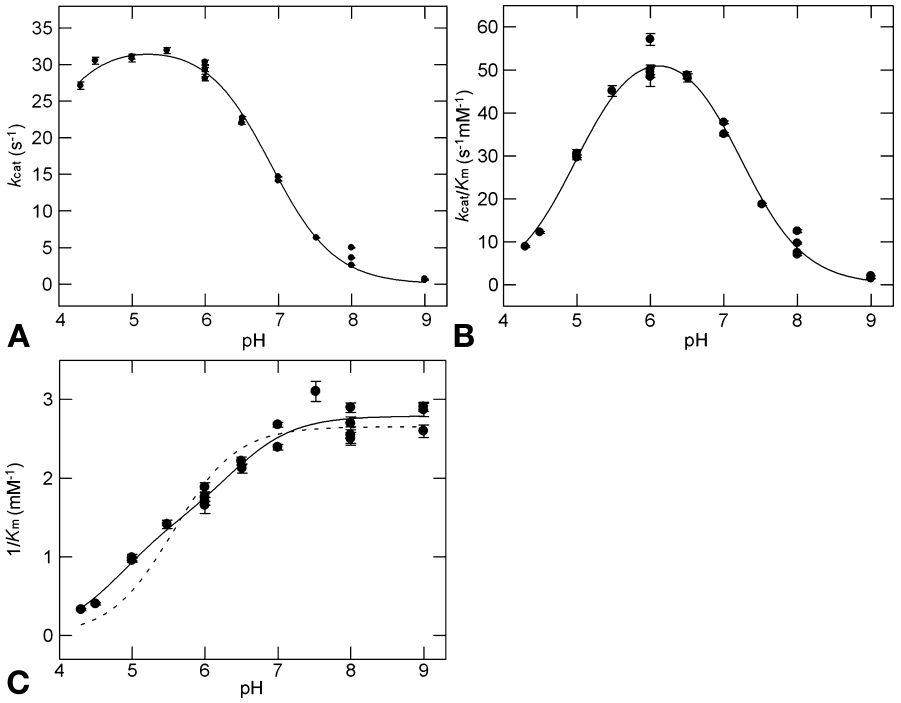


Fig. 7. Influence of pH on steady-state kinetic parameters of SXA-catalyzed hydrolysis of 4NPX. Initial-rate data, determined by using Method B, were fitted to Eq. 1 to determine kinetic parameters. Standard errors from fitting the data are indicated. **(A)** $k_{cat}$ vs pH. The curve was generated by fitting the $k_{cat}$ values for each pH to Eq. 5: pH-independent $k_{cat} = 32.7 \pm 0.5\ s^{-1}$, $pK_{a1} = 3.54 \pm 0.10$, $pK_{a2} = 6.90 \pm 0.03$. **(B)** $k_{cat}/K_m$ vs pH. The curve was generated by fitting the $k_{cat}/K_m$ values for each pH to Eq. 5: pH-independent $k_{cat}/K_m = 58.7 \pm 1.3\ s^{-1}mM^{-1}$, $pK_{a1} = 5.00 \pm 0.04$, $pK_{a2} = 7.23 \pm 0.04$. **(C)** $1/K_m$ vs pH. The solid curve was generated by fitting the data to Eq. 7 (two protonatable groups): middle limit $1/K_m = 1.46 \pm 0.33\ mM^{-1}$, upper limit $1/K_m = 2.79 \pm 0.06\ mM^{-1}$, $pK_{a1} = 4.81 \pm 0.21$, $pK_{a2} = 6.39 \pm 0.26$, reduced $\chi^2 = 0.0242$. The dotted curve was generated by fitting the data to Eq. 4 (single protonatable group): pH-independent $1/K_m = 2.65 \pm 0.081\ mM^{-1}$, $pK_a = 5.56 \pm 0.08$, reduced $\chi^2 = 0.0694$. F test indicates that there is a 0.022% probability that data fit Eq. 4 as well as Eq. 7.

$pK_a$ of D14 is shifted in the ES complex in comparison to the free enzyme ($pK_a = 5.0$) because in our models of SXA complexed with A2, X2, and AX (Fig. 2) there is space for only one water molecule in subsite –1. The water (water of hydrolysis) is located between substrate C1 and the carboxyl group of D14. Thus, in this model, the "diprotic" SXA ($D14^H$ $E186^H$) does not bind nor catalyze the hydrolysis of 4NPX nor 4NPA. On the basic side, differences between the two $k_{cat}$ profiles are likely conferred by formation of a nonproductive complex between substrate 4NPX and the "dianionic" form of SXA ($D14^-$ $E186^-$), in which both the general base and general acid are deprotonated and unable to catalyze the hydrolysis reaction, whereas substrate 4NPA does not bind to the "dianionic" form. The binding constant of 4NPX to the "dianionic" SXA is moderately more potent than the

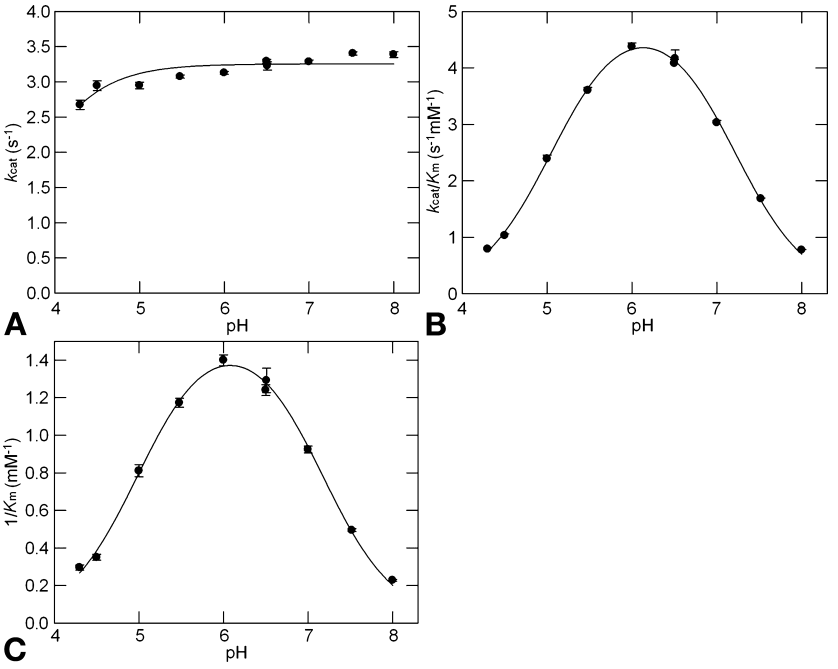


Fig. 8. Influence of pH on steady-state kinetic parameters of SXA-catalyzed hydrolysis of 4NPA. Initial-rate data, determined by using Method B, were fitted to Eq. 1 to determine kinetic parameters. Standard errors from fitting the data are indicated. **(A)** $k_{cat}$ vs pH. The curve was generated by fitting the $k_{cat}$ values for each pH to Eq. 4: pH-independent $k_{cat} = 3.25 \pm 0.05\ s^{-1}$, $pK_a = 3.64 \pm 0.10$. **(B)** $k_{cat}/K_m$ vs pH. The curve was generated by fitting the $k_{cat}/K_m$ values for each pH to Eq. 5: pH-independent $k_{cat}/K_m = 5.10 \pm 0.07\ s^{-1}mM^{-1}$, $pK_{a1} = 5.06 \pm 0.02$, $pK_{a2} = 7.20 \pm 0.02$. **(C)** $1/K_m$ vs pH. The curve was generated by fitting the data to Eq. 5: pH-independent $1/K_m = 1.60 \pm 0.02\ mM^{-1}$, $pK_{a1} = 5.00 \pm 0.03$, $pK_{a2} = 7.16 \pm 0.03$.

binding constant to the "monoanionic" SXA ($D14^- E186^H$), the latter in which the base and acid are in the correct protonation state for catalysis. Thus, increased pH inhibits the SXA-catalyzed hydrolysis of 4NPX noncompetitively (inhibition cannot be overcome by increased 4NPX concentrations) and the $1/K_m$(4NPX) value remains high, but the SXA-catalyzed hydrolysis of 4NPA is inhibited competitively by increased pH so that $k_{cat}$ remains at the pH-independent value as $1/K_m$(4NPA) becomes smaller.

The pH dependency of $1/K_m$(4NPX) fits a diprotic model (Eq. 7) with two protonatable groups on the acidic limb (Fig. 7C): $pK_{a1} = 4.8$ and $pK_{a2} = 6.4$. In the diprotic model, 4NPX binds with ~2-fold greater affinity to the "dianionic" SXA ($D14^- E186^-$) than to the "monoanionic" SXA ($D14^- E186^H$), and it does not bind to the "diprotic" form of enzyme ($D14^H E186^H$). The parameter, $1/K_m$(4NPX), can be fitted to a monoprotic model (Eq. 4), but the fitted curve has a higher reduced $\chi^2$ value than that for the diprotic model (Eq. 7) and F test indicates that there is 0.022% probability the data fit Eq. 4 as well as Eq. 7 (Fig. 7C). Also, fitting the data to Eq. 4 provides $pK_a$ value

of 5.6 for $1/K_m$(4NPX), which approximates an average of the values for $pK_{a1}$ and $pK_{a2}$, determined in the diprotic model, and $pK_a$ of 5.6 has no known structure–function relevance.

It is not unusual, in the literature, for the relative activities of bifunctional enzymes to be reported as a ratio of the two individual activities, measured separately at a single pH and single substrate concentration. In the case of SXA, which has disparate pH profiles for $k_{cat}$ with substrates 4NPX and 4NPA, relative rates (4NPX/4NPA) at a single pH and nearly saturating substrate concentrations would range from 10 to 0.6 between pH 4.3 and 8.0 and would approach 0 at higher pHs. The different pH profiles for $1/K_m$ and $k_{cat}$ for substrates 4NPX and 4NPA could lead to an incorrect inference that SXA has separate active sites for the two substrates; this, of course, can be ruled out from our data that indicates mutations of SXA active-site residues (D14A and E186A), which impart severe erosion of catalysis, have similar values as wild-type SXA for relative substrate specificities of 4NPX and 4NPA: $k_{cat}/K_m$(4NPX)/$k_{cat}/K_m$(4NPA) = 12 at pH 5.3 and 25°C.

## Conclusions

SXA is the best catalyst known for promoting hydrolysis of β-d-1,4-xylooligosaccharides, by factors greater than 15 when comparing $k_{cat}$ and $k_{cat}/K_m$ values for substrates X2-X6 to values obtained for the enzymes from other species. This property, its ability to catalyze hydrolysis of arabinoxylose *(13)*, its favorable pH optima (nearly constant $k_{cat}$ between pH 4.5 and 6.0), and its apparent lack of transglycosylation activity place SXA in the forefront among β-xylosidases for application in the saccharification of xylan-containing materials. Limitations to its effectiveness, if any, in fermentation applications can be addressed upon their identification. SXA was isolated from an organism, *S. ruminantium,* whose native environment (cow rumen) is rich in materials containing xylan and (with assistance from xylanases) xylooligosaccharides. Thus, SXA serves in a high-throughput environment that may select for high performing catalysts in providing nutrients to support the large animal. It is encouraging that diversity of hydrolases in the cow rumen continues to be explored *(29)*.

Certain mechanistic fundamentals are established for SXA: it catalyzes hydrolysis of the glycosidic bond shared by the terminal residue of the nonreducing end of substrate, SXA catalyzes hydrolysis through a single displacement mechanism that inverts the configuration of the anomeric carbon that shares the glycosidic bond of hydrolysis, the catalytic base and catalytic acid of SXA have $pK_a$ values of approx 5 and 7, respectively, hydrolysis of 4NPX and 4NPA are catalyzed by the same active site with the sugar moiety occupying subsite –1, and subsites –1 and +1 are the only subsites that affect binding and catalysis. Subsites –1 and +1 can exert considerable and selective catalytic power as seen in the progression of relative $k_{cat}$ values (at pH 5.3 and 25°C) of 5600, 340, 34, and 1 for substrates X2, 4NPX, 4NPA, and A2, respectively.

Biochemical conclusions are fully consistent with the three-dimensional models of the active site in terms of residues and distances: the active-site models allow assignments of D14 and E186 as the catalytic base and catalytic acid, respectively; the lack of subsites beyond –1 on the nonreducing side owe to the active site being capped with amino acid residues that prevent formation of additional subsites; the lack of subsites beyond +1 on the reducing side owes to the wide, solvent-exposed opening to the active site preventing additional subsites to be defined; and the $pK_a$ values for the carboxyl groups of D14 and E186 are differentially modulated through H bonds and a salt bridge. In addition, the models place restrictions on the binding mode of putative substrate AX (arabinose moiety must occupy subsite –1) and arabinoxylose analogs that may serve as substrates.

The influence of pH on catalysis apparently reflects the protonation state of the catalytic base (D14, $pK_a = 5.0$ for $k_{cat}/K_m$) and catalytic acid (E186, $pK_a = 7.2$ for $k_{cat}/K_m$). The catalytically active form of SXA is the "monoanionic" form ($D14^- E186^H$). One of the two catalytically inactive forms of SXA is the "diprotonated" form ($D14^H E186^H$). $D14^H E186^H$ binds substrates 4NPX and 4NPA weakly, if at all, because otherwise the pH profiles for $k_{cat}$ would reflect a $pK_a$ of 5, which they do not. Thus, $D14^H E186^H$ has no apparent functional properties. It is plausible that the protonation state of $D14^H E186^H$ disrupts H bonds and the salt bridge that are formed in the active site of $D14^- E186^H$ such that ligand recognition elements are dismantled. The other catalytically inactive form of SXA is the "dianionic" form ($D14^- E186^-$). $D14^- E186^-$ binds 4NPA weakly, if at all, but it binds 4NPX with approximately twofold greater affinity than the $D14^- E186^H$ enzyme. We speculate that $D14^- E186^-$ may bind the xylose residue of 4NPX in subsite +1 (or portions thereof) to avoid clash between the negative charges of the carboxylic acids (belonging to D14 and E186) in subsite –1 and the oxygen atoms of the sugar moiety. Certainly, subsite +1 has affinity for D-xylose as seen in the 13-fold larger $k_{cat}$ and 2-fold larger $k_{cat}/K_m$ of SXA acting on X2 in comparison to 4NPX. Subsite +1 of SXA may have little or no affinity for arabinofuranose, as suggested by the 36-fold larger $k_{cat}$ and 13-fold larger $k_{cat}/K_m$ of SXA acting on 4NPA in comparison to A2. Repulsion of 4NPA from subsite –1 of the $D14^- E186^-$ enzyme, without binding affinity for subsite +1 to form a nonproductive complex, would account for the pH independence of $k_{cat}$ above pH 4 for SXA acting on 4NPA. In any case, the catalytically inactive $D14^- E186^-$ has ligand binding properties, which distinguish it from the apparently functionless $D14^H E186^H$.

## Acknowledgments

We thank Jay D. Braker and Patrick Kane for excellent technical assistance in contributing to this work. We thank Dr. Peter Biely for generously providing a sample of 4NPX2.

## References


1. Saha, B. C. (2003), *J. Ind. Microbiol. Biotechnol.* **30,** 279–291.
2. Zechel, D. L., and Withers, S. G. (2001), *Curr. Opin. Chem. Biol.* **5,** 643–649.
3. Sinnott, M. L. (1990), *Chem. Rev.* **90,** 1171–1202.
4. Herrmann, M. C., Vrsanska, M., Jurickova, M., Hirsch, J., Biely, P., and Kubicek, C. P. (1997), *Biochem. J.* **321,** 375–381.
5. Marshall, P. J., and Sinnott, M. L. (1983), *Biochem. J.* **215,** 67–74.
6. Shallom, D., Leon, M., Bravman, T., Ben-David, A., Zaide, G., Belakhov, V., Shoham, G., Schomburg, D., Baasov, T., and Shoham, Y. (2005), *Biochemistry* **44,** 387–397.
7. Vocadlo, D. J., Wicki, J., Rupitz, K., and Withers, S. G. (2002), *Biochemistry* **41,** 9727–9735.
8. Bravman, T., Zolotnitsky, G., Belakhov, V., Shoham, G., Henrissat, B., Baasov, T., and Shoham, Y. (2003), *Biochemistry* **42,** 10,528–10,536.
9. Lee, R. C., Hrmova, M., Burton, R. A., Lahnstein, J., and Fincher, G. B. (2003), *J. Biol. Chem.* **278,** 5377–5387.
10. Cotta, M. A. (1993), *Appl. Environ. Microbiol.* **59,** 3557–3563.
11. Williams, A. G., Withers, S. E., and Joblin, K. N. (1991), *Lett. Appl. Microbiol.* **12,** 232–235.
12. Cotta, M. A., and Whitehead, T. R. (1998), *Curr. Microbiol.* **36,** 183–189.
13. Whitehead, T. R., and Cotta, M. A. (2001), *Curr. Microbiol.* **43,** 293–298.
14. Barshop, B. A., Wrenn, R. F., and Frieden, C. (1983), *Anal. Biochem.* **130,** 134–145.
15. Guex, N., and Peitsch, M. C. (1997), *Electrophoresis* **18,** 2714–2723.
16. Pettersen, E. F., Goddard, T. D., Huang, C. C., Couch, G. S., Greenblatt, D. M., Meng, E. C., and Ferrin, T. E. (2004), *J. Comput. Chem.* **25,** 1605–1612.
17. Sanner, M. F., Olson, A. J., and Spehner, J. C. (1996), *Biopolymers* **38,** 305–320.
18. Gill, S. C., and von Hippel, P. H. (1989), *Anal. Biochem.* **182,** 319–326.
19. Kezdy, F. J., and Bender, M. L. (1962), *Biochemistry* **1,** 1097–1106.
20. Nurizzo, D., Turkenburg, J. P., Charnock, S. J., Roberts, S. M., Dodson, E. J., McKie, V. A., Taylor, E. J., Gilbert, H. J., and Davies, G. J. (2002), *Nat. Struct. Biol.* **9,** 665–668.
21. Davies, G. J., Wilson, K. S., and Henrissat, B. (1997), *Biochem. J.* **321,** 557–559.
22. Kersters-Hilderson, H., Claeyssens, M., Van Doorslaer, E., and De Bruyne, C. K. (1976), *Carbohydr. Res.* **47,** 269–273.
23. Braun, C., Meinke, A., Ziser, L., and Withers, S. G. (1993), *Anal. Biochem.* **212,** 259–262.
24. Van Doorslaer, E., Kersters-Hilderson, H., and De Bruyne, C. K. (1985), *Carbohydr. Res.* **140,** 342–346.
25. Wagschal, K, Franqui-Espiet, D., Lee, C. C., Robertson, G. H., and Wong, D. W. (2005), *Appl. Environ. Microbiol.* **71,** 5318–5323.
26. Kimura, I., and Tajima, S. (1999), *J. Biosci. Bioeng.* **87,** 572–575.
27. Wolfenden, R., Lu, X., and Young, G. (1998), *J. Am. Chem. Soc.* **120,** 6814–6815.
28. Cleland, W. W. (1982), *Methods Enzymol.* **87,** 390–405.
29. Ferrer, M., Golyshina, O. V., Chernikova, T. N., Khachane, A. N., Reyes-Duarte, D., Martins Dos Santos, V. A. P., Strompl, C., Elborough, K., Jarvis, G., Neef, A., Yakimov, M. M., Timmis, K. N., and Golyshin, P. N. (2005), *Environ. Mircobiol.* **7,** 1996–2010.